Supplemental Material: Thermal Fracture Kinetics of Heterogeneous Semiflexible Polymers

Alexander Lorenzo,[1] Enrique M. De La Cruz,[2] and Elena F. Koslover[1,*]

[1] *Department of Physics, University of California, San Diego, San Diego, California 92093*
[2] *Department of Molecular Biophysics and Biochemistry, Yale University, New Haven, CT 06520*

(Dated: January 21, 2020)

APPENDIX

A. ANGULAR DYNAMICS FOR COUPLED RIGID LINKS

In this section we derive the angular dynamics for two connected rigid links, each of length ℓ, in a highly viscous fluid. We assume each of the links has a friction coefficient per unit length μ, and that there is a bending modulus κ for the junction between the links. This simplified system serves as a basis for deriving the appropriate dynamics of the junction angle for the heterogeneous worm-like chain.

We define a given configuration of the system by the center of mass positions for the two rigid rods $(\vec{r}_1, \vec{r}_2)$ and their normalized orientations $(\vec{u}_1, \vec{u}_2)$. The overall energy for this configuration is then given by,

$$E = \kappa(1 - \vec{u}_1 \cdot \vec{u}_2) + \vec{\lambda} \cdot \left(\vec{r}_1 + \frac{\ell}{2} u_1 - \vec{r}_2 + \frac{\ell}{2} \vec{u}_2 \right). \quad \text{(S1)}$$

Here, the first term corresponds to the bending energy of the junction between the two rods and the second term uses a Lagrange multiplier $(\vec{\lambda})$ to enforce the connectivity of the two inextensible rods at the junction.

In the freely draining approximation, and in the absence of Brownian forces, the overdamped dynamics of such a system are defined by the equations,

$$\begin{aligned} \zeta_r \vec{\omega}_i &= -\vec{u}_i \times \frac{\partial E}{\partial u_i} \\ \zeta_t \frac{d\vec{r}_i}{dt} &= -\frac{\partial E}{\partial \vec{r}_i}, \end{aligned} \quad \text{(S2)}$$

where $\vec{\omega}_i$ gives the rotational velocity for each rod $(i = 1, 2)$. Here, $\zeta_r = \mu\ell^3/12$ is the rotational frictional coefficient of each rod around its center of mass and $\zeta_t = \mu\ell$ the translational friction coefficient[1]. The Lagrange multiplier $\vec{\lambda}$ can be obtained from the constraints:

$$\begin{aligned} \frac{d}{dt}\left(\vec{r}_1 + \frac{\ell}{2} u_1 - \vec{r}_2 + \frac{\ell}{2} \vec{u}_2 \right) \cdot \vec{u}_1 = 0 \\ \frac{d}{dt}\left(\vec{r}_1 + \frac{\ell}{2} u_1 - \vec{r}_2 + \frac{\ell}{2} \vec{u}_2 \right) \cdot \vec{u}_2 = 0. \end{aligned} \quad \text{(S3)}$$

Solving these equations yields $\vec{\lambda} \cdot \vec{u}_i = \frac{6\kappa(1-\rho^2)}{\ell(5-3\rho)}$, where $\rho = \vec{u}_1 \cdot \vec{u}_2$. The dynamics of the angular coordinate ρ are then given by,

$$\frac{d\rho}{dt} = \frac{48\kappa(1-\rho^2)}{\mu\ell^3(5-3\rho)}. \quad \text{(S4)}$$

This expression gives the effective friction coefficient for the coordinate ρ according to

$$\begin{aligned} \frac{d\rho}{dt} &= -\frac{1}{\zeta(\rho)} \frac{\partial E_{\text{bend}}}{\partial \rho} = -\frac{\kappa}{\zeta(\rho)} \\ \zeta(\rho) &= \frac{\mu\ell^3(5-3\rho)}{48(1-\rho^2)} = \frac{k_B T}{D_\rho^{(0)}} \frac{5-3\rho}{6(1-\rho^2)} \end{aligned} \quad \text{(S5)}$$

where $D_\rho^{(0)}$ is the effective diffusivity along the ρ coordinate.

For the angular dynamics of a junction in a continuum worm-like chain, changes in the angle require dragging along a length of chain that should scale as the junction size Δ. We select an effective link length $\ell = 2\Delta$ for use in Eq. 7. The prefactor of 2 is obtained from fitting to Brownian dynamics simulations with fixed end-to-end distance (as shown in Fig. 2a). This is the only fitting parameter in the theory and is used for all results shown in subsequent figures.

The dynamic prefactor $D_\rho^{(0)}$ for movement along the ρ coordinate describes the rapid dynamics of the short chain length represented by the junction region. Consequently, this prefactor is dependent only on the length scale Δ and not on the total chain length. In Supplemental Fig. S1 we show a comparison between Brownian dynamics simulations and the approximate kinetic model for two different chain lengths, showing that the same prefactor $D_\rho^{(0)}$ is applicable regardless of chain length. We note that for a fixed normalized end-to-end distance r, the mean first passage time to a cutoff junction energy over the ρ coordinate is higher for a longer chain. This effect is due to the fact that the landscape for a fixed r is flatter for a long chain, leading to a slower approach down the free energy hill towards steeper junction angles. This comparison thus highlights that the kinetics in ρ are fundamentally distinct from Kramers' transition state theory, as they involve sliding down towards a free energy valley rather than transition over an energy barrier.

* ekoslover@ucsd.edu

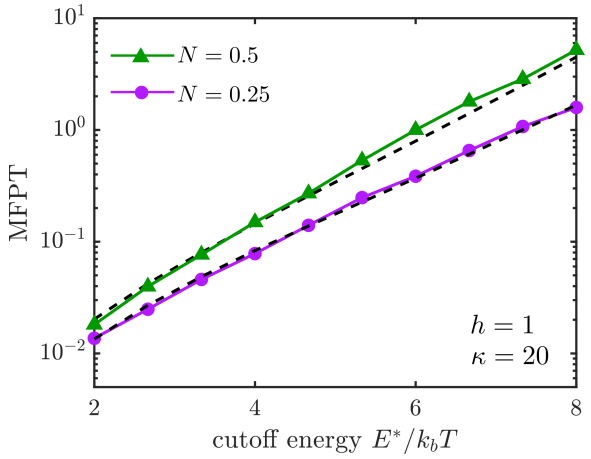

Figure S1. Comparison of approximate dynamics over free energy landscape vs Brownian dynamics simulations, for two different chain lengths. The mean first passage time to a cutoff junction energy E^* is plotted for a fixed normalized end-to-end distance $r = R/(2L) = 0.5$, for a chain of dimensionless length $N = 0.25$ and one of length $N = 0.5$. The same junction size $\Delta = \ell_{p,1}/\kappa$ and same dynamic prefactor $D_\rho^{(0)}$ (Eq. 7) is used for both chains.

B. MEAN FIRST PASSAGE TIME ON A 1D LANDSCAPE

For one-dimensional systems with spatially varying diffusivity $D(x)$ and free energy landscape $F(x)$, it has been shown that the Fokker-Planck equation which correctly reproduces the Boltzman distribution in the steady state[2] is given by,

$$\frac{dG(x,t|x_0)}{dt} = \frac{\partial}{\partial x}\left[D(x)\left(\frac{1}{kT}\frac{\partial F}{\partial x}G + \frac{\partial G}{\partial x}\right)\right] \tag{S6}$$

where $G(x,t|x_0)$ is the Green's function giving the distribution over x at time t for a system that started at position x_0. A corresponding backward Kolmogorov equation can be derived for this system[3] as,

$$\frac{dG}{dt} = \left[-\frac{D(x_0)}{kT}\frac{\partial F}{\partial x_0} + \frac{\partial D}{\partial x_0}\right]\frac{\partial G}{\partial x_0} + D(x_0)\frac{\partial^2 G}{\partial x_0^2} \tag{S7}$$

Assuming the system has an absorbing boundary at a and a reflecting boundary at L, the mean first passage time is defined based on the probability $Q(t|x_0) = \int_a^L G(x,t|x_0)dx$ that the absorbing boundary has not yet been reached. Namely, the MFPT is given by $T(x_0) = -\int_0^\infty t\frac{dQ}{dt}$. We solve for $T(x_0)$ using Eq.S7 in a manner analogous to previous calculations with a constant diffusivity[4, 5]. Assuming an equilibrated distribution of starting positions, the overall mean first passage time is then given by

$$\langle T\rangle = \frac{1}{\int_0^L e^{-F(x)/kT}dx}\times \times\left[\int_a^L dx\int_a^x dy\int_y^L dz\,\frac{1}{D(y)}e^{(F(y)-F(z)-F(x))/kT}\right] \tag{S8}$$

The expression in Eq. S8 matches that derived in the classic paper by Szabo, Schulten, and Schulten[6], modified for a starting position distributed according to thermal equilibrium, with first passage times set to zero for those trajectories that start below the absorbing boundary at a. We use numerical integration of Eq. S8 to calculate the mean first passage time for each fixed value of r over the energy landscape plotted in Fig. 1.

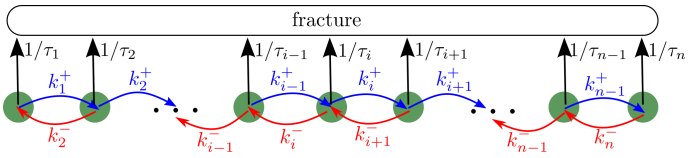

Figure S2. Schematic of discrete state model for dynamics of the chain ends. Each state (green circle) corresponds to a particular chain end separation (r_i), and has a specific timescale for fracture (τ_i). Transition rates between states ($k_i^\pm$) are defined by Eq. 9. For calculations of first passage time to a given end separation (Fig. 2B), the fracture state and all r_i below a particular cutoff r^* are removed from the model.

C. MEAN FIRST PASSAGE TIME ON A DISCRETIZED LANDSCAPE

We consider the calculation of mean first passage time on a discretized landscape consisting of a network of states with well-defined transition rates between them. This approach for calculating low-order moments of transition times is well established in the field of network theory[7]. Similar approaches have also been extensively employed in the study of molecular dynamics over complex landscapes, under the names of "discrete path sample"[8] and "Markov State Models"[9]. Here, for convenience, we reproduce the derivation of the MFPT specifically for our system of interest. Our derivation follows the same approach as described in prior work on kinetics with state-dependent rates[10].

Consider a network of states, with each state (r_i, for $i = 1,\ldots,n$) corresponding to a different separation of the chain ends. The transitions between neighboring states are treated as memory-less Poisson processes with rate constants $k_i^\pm$ (given by Eq. 9). From each state, there is another Poisson transition available to a fractured state, with rate constant τ_i (calculated via Eq. 8). A schematic of this system is presented in Fig. S2.

Two versions of this system are used in our manuscript. In the first (for the calculations in Fig. 2b), the junction bending is ignored ($\tau_i \to \infty$), and we are interested specifically in the transition time to a particular end-to-end separation (state r_*). In the second (calculations for Fig. 2c and Fig. 4), the system is allowed to fluctuate over all r_i states and we are interested in the first passage time to the fractured state. The same mathematical formalism can be used for both cases.

We define $P_{i,j}(t)$ as the transition time distribution between state i and a neighboring state j and $Q_i(t)$ as the probability the system has not yet left state i after arriving there. For the Poisson processes used here,

$$\begin{aligned} Q_i(t) &= e^{-(k_i^+ + k_i^- + 1/\tau_i)t} \\ P_{i,i\pm1}(t) &= k_i^{\pm} Q_i(t) \end{aligned} \tag{S9}$$

We can then calculate the cumulative probability $H_i(t)$ that the system has not yet reached fracture, given that it started in state i at time 0. This probability is given by:

$$H_i(t) = Q_i(t) + \sum_{j=1}^{n} \sum_{m=0}^{\infty} \sum_{i \xrightarrow{m} j} P_{ik_1} * P_{ik_2} \ldots * P_{k_m j} * Q_{ji}, \tag{S10}$$

where the summation is over all final states j, and all paths of length m to get from state i to state j, and the $*$ refer to convolution.

A Laplace transform in time ($\widehat{H}_i(s) = \mathcal{L}[H_i(t)]$, etc) converts the convolutions to a product over the propagators P_{ij}, giving the vectorized expression

$$\widehat{\mathbf{H}} = \widehat{\mathbf{Q}} + \sum_{m=0}^{\infty} \widehat{\mathbf{P}}^m \cdot \widehat{\mathbf{Q}} \tag{S11}$$

where $\widehat{\mathbf{P}}$ is a matrix with entries $\widehat{P}_{ij}$, $\widehat{\mathbf{Q}}$ a vector with entries $\widehat{Q}_i$ and $\widehat{\mathbf{H}}$ a vector with entries $\widehat{H}_i$. Simplifying the geometric series then yields

$$\widehat{\mathbf{H}} = (\mathbf{I} - \widehat{\mathbf{P}})^{-1} \cdot \widehat{\mathbf{Q}}$$

The mean first passage time to fracture, starting from state i, is calculated as

$$\mathrm{MFPT}_i = \int_0^\infty t \left[-\frac{dH_i(t)}{dt} \right] dt = \widehat{H}_i(s=0) \tag{S12}$$

Finally, we average over starting position i with the appropriate equilibrium Boltzman distribution of starting probabilities in the different states. For the case of transition to a particular r^* cutoff, the same approach is applied except that all states below r^* are removed from the system.

We note that this approach relies on a discretization of the r coordinate, enabling us to separately calculate a fracture time τ_i for each discrete state. The discretization δr was taken to be sufficiently small that the final results were independent of discretization value, as shown in Fig. S3.

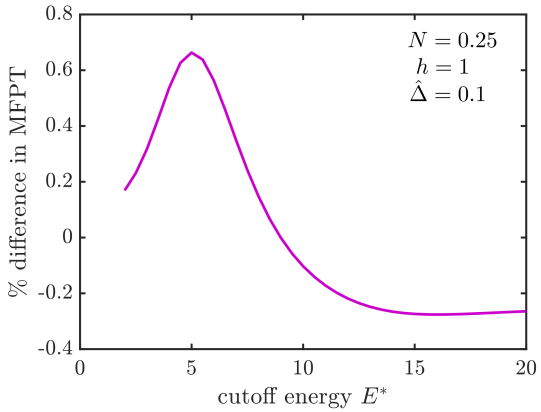

Figure S3. Landscape discretization in the r coordinate has little effect on calculated MFPT to fracture. Plotted is the percentage difference in MFPT for a discretization of $\delta r = 0.01$ versus $\delta r = 0.04$, as a function of the junction cutoff energy E^*. The MFPT is calculated as for Fig. 2c. The two discretizations give results that differ by less than 1%.

D. BROWNIAN DYNAMICS SIMULATIONS

Brownian dynamics simulations are used to verify our simplified model for dynamics over a free energy landscape in the ρ and r coordinates. We define a discretized version of the heterogeneous worm-like chain model, using the standard bead-rod formalism [11], with very stiff stretching modulus for constraining the length of the rods. Our chains consist of $n = 20$ segments of length d, with bending energy

$$\frac{1}{k_B T} E_{\mathrm{bend}} = \sum_{i=1}^{n-1} \kappa_i \left[1 - \cos(\rho_i)\right] \tag{S13}$$

for $\rho_i = \cos\theta_i$ and θ_i the angle between orientations of each consecutive pair of segments. The prefactor is set to $\kappa_i = \frac{\ell_{p,1}}{d}$ for $i \leq 10$ and $\kappa_i = \frac{\ell_{p,2}}{d}$ otherwise. The central bead represents a junction of size $\Delta = d$.

Chains are initiated in a thermally equilibrated configuration by direct sampling of the segment angles. A standard Brownian dynamics algorithm [12] with 4th-order Runge-Kutta time integration[13] is used to propagate the system forward in timesteps of $\delta t = 10^{-4} \frac{d^2 \mu_b}{k_B T}$, where the μ_B is the friction coefficient of each bead. Simulations are run until either the chain angle at the 10th bead (ρ_9) or the end-to-end distance reaches a cutoff value, up to a maximum of 10^7 timesteps.

Mean first passage times to cutoff cannot be obtained by direct averaging since many chains to not reach the cutoff over the simulation time. Instead, we fit the empirical cumulative distribution function for first passage times to the functional form $1 - \exp(-t/\tau)$, to extract the appropriate time-scale for first passage. 10^4 chains are simulated for each data point plotted in Fig. 2.

In addition to simulations with homogeneous chains,

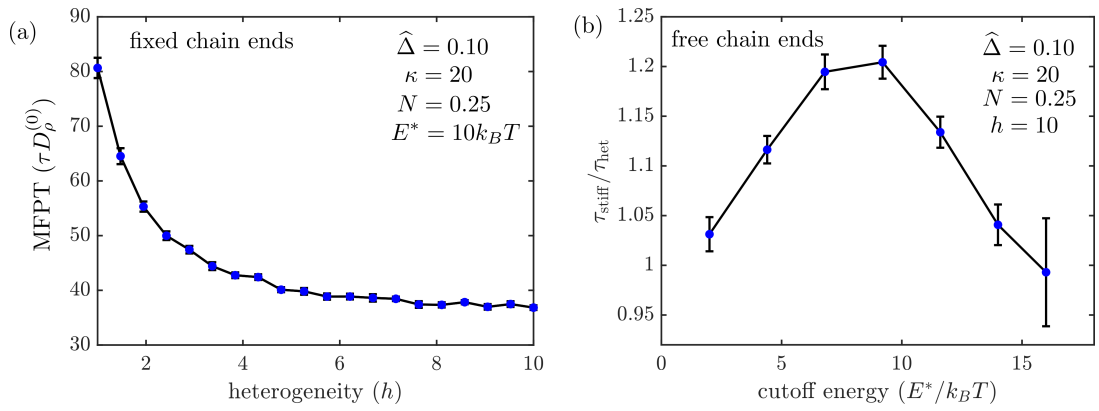

Figure S4. Transition times in BD simulations with heterogeneous chains. (a) Starting chain configurations were selected from an equilibrium distribution, and chain ends were held fixed throughout the simulation. Mean first passage times to a junction energy cutoff of $E^* = 10k_bT$ is shown as a function of chain heterogeneity. Qualitative trend is comparable to analytical calculations in Fig. 3b. (b) Simulations with free chain ends, for a fixed heterogeneity of $h = 10$ (heterogeneous chain) or $h = 1$ (homogeneously stiff chain). The ratio of MFPT for the homogeneous and heterogeneous chain is plotted for different cutoff junction energies. Qualitative trend is comparable to analytical calculations in Fig. 4. Parameters used in the simulations were $N = 0.25, \kappa = 20k_bT, \widehat{\Delta} = 0.1$. Error bars are standard errors obtained from a bootstrapping (100 bootstrapping replicates generated for each point).

Brownian dynamics simulations of chains with heterogeneity up to $h = 10$ are shown in Supplemental Fig. S4. Chains of length 20 segments (21 beads) were simulated and mean first passage times extracted as described above. The junction was defined as the last bead located wholly on the stiff side of the chain (bead 10). Because simulations cannot access the very rare transition events associated with high junction energy cutoffs, we used a lower cutoff energy ($E^* = 10k_BT$) for chains with fixed end positions. Initial simulation configurations were selected from an equilibrium distribution. The resulting transition times (Fig. S4a) show the same qualitative dependence on chain heterogeneity as seen with the kinetic model (Fig. 3b,c).

Similarly, we carried out simulations of highly heterogeneous ($h = 10$) and homogeneous ($h = 1$) chains where the chain ends were free to move throughout the simulation (Supplemental Fig. S4b). These simulations also exhibit the same qualitative behavior as predicted by our approximate kinetic model (Fig. 4): a modest speed-up in the first passage time is obtained for heterogeneous chains over homogeneous chains with free ends. This speed-up is evident primarily at intermediate cutoff energies, where the junction has to bend substantially to achieve the cutoff but the transition still happens relatively fast compared to the equilibration of the chain ends. It should be noted that these simulations are very coarse-grained, with the soft side persistence length having a value not much longer than individual segment lengths ($\ell_{p,2} = 2d$). Hence, the behavior of the soft side of the chain is not fully resolved, which may account for the slight quantitative shift in the ratio of transition times when compared with kinetic model calculations (Fig. 4).

The similarity between simulation results and the approximate kinetic model helps substantiate the primary result of our manuscript – the phenomenon that chain heterogeneity can enhance fracture at a localized junction region.

E. CAPTIONS FOR SUPPLEMENTAL VIDEOS

- **Supplemental Video 1:** Snapshots of Brownian dynamics simulation for a homogeneously stiff chain with $N = 0.25$, $\widehat{\Delta} = 0.1$, and $h = 1$. The last 300 frames of a trajectory ending in fracture ($E^* = 16k_BT$) are shown, with the corresponding positions on the energy landscape (From Fig. 1b) indicated. Junction color corresponds to the bending energy at the junction ($E_{\rm junc}$; beige for low energy, red for high energy). The closer approach of the chain ends as the junction bends can be seen towards the end of the video.

- **Supplemental Video 2:** Snapshots of Brownian dynamics simulation for a heterogeneous stiff chain with $N = 0.25$, $\widehat{\Delta} = 0.1$, and $h = 10$. The last 300 frames of a trajectory ending in fracture ($E^* = 16k_BT$) are shown, with the corresponding positions on the energy landscape (From Fig. 1d) indicated. Junction color corresponds to the bending energy at the junction ($E_{\rm junc}$; beige for low energy, red for high energy).

[1] M. Doi and S. F. Edwards, *The theory of polymer dynamics*, volume 73, Oxford University Press, 1988.

[2] A. W. Lau and T. C. Lubensky, Phys Rev E **76**, 011123 (2007).

[3] H. Risken, Fokker-planck equation, in *The Fokker-Planck Equation*, pages 63–95, Springer, 1996.

[4] R. F. Fox, Phys Rev A **33**, 467 (1986).

[5] E. F. Koslover and A. J. Spakowitz, Phys Rev Lett **102**, 178102 (2009).

[6] A. Szabo, K. Schulten, and Z. Schulten, The Journal of chemical physics **72**, 4350 (1980).

[7] N. Masuda, M. A. Porter, and R. Lambiotte, Physics reports **716**, 1 (2017).

[8] D. J. Wales, Molecular physics **100**, 3285 (2002).

[9] J. D. Chodera and F. Noé, Current opinion in structural biology **25**, 135 (2014).

[10] E. F. Koslover and A. J. Spakowitz, Phys Rev E **86**, 011906 (2012).

[11] M. Somasi, B. Khomami, N. J. Woo, J. S. Hur, and E. S. Shaqfeh, J Non-newton Fluid **108**, 227 (2002).

[12] D. L. Ermak and J. McCammon, J Chem Phys **69**, 1352 (1978).

[13] E. F. Koslover and A. J. Spakowitz, Phys Rev E **90**, 013304 (2014).